Available online at www.sciencedirect.com
ScienceDirect
Journal of Power Sources 164 (2007) 56–64
JOURNAL OF POWER SOURCES
www.elsevier.com/locate/jpowsour

Fabrication and characterization of a co-fired $La_{0.6}Sr_{0.4}Co_{0.2}Fe_{0.8}O_{3-\delta}$ cathode-supported $Ce_{0.9}Gd_{0.1}O_{1.95}$ thin-film for IT-SOFCs

Y. Liu *, S. Hashimoto, H. Nishino, K. Takei, M. Mori

Materials Science Research Laboratory, Central Research Institute of Electric Power Industry, 2-6-1 Nagasaka, Yokosuka-shi, Kanagawa-ken 240-0196, Japan

Received 19 October 2006; accepted 26 October 2006
Available online 30 November 2006

Abstract

A dense membrane of $Ce_{0.9}Gd_{0.1}O_{1.95}$ on a porous cathode based on a mixed conducting $La_{0.6}Sr_{0.4}Co_{0.2}Fe_{0.8}O_{3-\delta}$ was fabricated via a slurry coating/co-firing process. With the purpose of matching of shrinkage between the support cathode and the supported membrane, nano-$Ce_{0.9}Gd_{0.1}O_{1.95}$ powder with specific surface area of 30 $m^2\,g^{-1}$ was synthesized by a newly devised coprecipitation to make the low-temperature sinterable electrolyte, whereas 39 $m^2\,g^{-1}$ nano-$Ce_{0.9}Gd_{0.1}O_{1.95}$ prepared from citrate method was added to the cathode to favor the shrinkage for the $La_{0.6}Sr_{0.4}Co_{0.2}Fe_{0.8}O_{3-\delta}$. Bi-layers consisting of <20 μm dense ceria film on 2 mm thick porous cathode were successfully fabricated at 1200 °C. This was followed by co-firing with NiO–$Ce_{0.9}Gd_{0.1}O_{1.95}$ at 1100 °C to form a thin, porous, and well-adherent anode. The laboratory-sized cathode-supported cell was shown to operate below 600 °C, and the maximum power density obtained was 35 mW cm^{-2} at 550 °C, 60 mW cm^{-2} at 600 °C.

Keywords: Solid oxide fuel cells; Cathode-supported SOFC; $La_{0.6}Sr_{0.4}Co_{0.2}Fe_{0.8}O_{3-\delta}$; Gadolinium-doped ceria oxide; Co-firing

1. Introduction

Lowering the operating temperature of solid oxide fuel cells (SOFCs) requires reduction of the thickness of the electrolyte by lowering the ohmic losses and/or the use of materials with faster ionic transport and higher catalytic activities [1]. Doped ceria has been considered to be a promising alternative to yttria stabilized zirconia (YSZ) or scandia stabilized zirconia (ScSZ), as its oxide-ionic conductivity is much higher in the low-temperature range [2–4]. The wide use of ceria is somewhat retarded because ceria electrolytes are reduced at low oxygen partial pressures (P_{O_2}) at the elevated temperatures and thereby create undesirable electronic conductivity and volumetric expansion [4–6]. Some reports have suggested that optimization of the doped species or operations may alleviate such dilemma to some degree [7–10]. Sintered ceria electrolytes are required to possess densities greater than 95% of theoretical in order to exclude open porosity and avoid reactant crossover. Although a higher sintering temperature yields a ceria of higher density, it tends to also produce micro-cracks, e.g. due to oxygen release caused by reduction of CeO_2 to Ce_2O_3, and poor mechanical stability as a result of formation of a microstructure with a grain size in the micron range [11–15]. This makes it necessary to develop a low-temperature sinterable ceria.

In addition to the electrolyte, an approach to improve the low-temperature performance of SOFCs involves replacement of the conventional $La_{1-x}Sr_xMnO_{3-\delta}$ cathode with one of mixed conductivity. As such promising classes, $La_{1-x}Sr_xCo_yFe_{1-y}O_{3-\delta}$ doped perovskites based on $LaCoO_3$ have attracted considerable attention [16]. The most common composition, $La_{0.6}Sr_{0.4}Co_{0.2}Fe_{0.8}O_{3-\delta}$, exhibits nonstoichiometry at high temperatures and at low P_{O_2} and displays a high oxygen surface and tracer diffusion coefficients. It has a high electrical conductivity of 350–400 S cm^{-1} at 500–600 °C and a high catalytic activity for oxygen reduction [17–19]. $La_{0.6}Sr_{0.4}Co_{0.2}Fe_{0.8}O_{3-\delta}$ was found to be chemically and thermally compatible with a doped ceria electrolyte giving a very low electrode/electrolyte resistance [20–22]. Many successful examples have made $La_{0.6}Sr_{0.4}Co_{0.2}Fe_{0.8}O_{3-\delta}$ and doped ceria a promising combination for low-temperature SOFC operation [23–25]. However,

* Corresponding author. Tel.: +81 46 856 2121; fax: +81 46 856 5571.
E-mail address: yu@criepi.denken.or.jp (Y. Liu).

0378-7753/$ – see front matter © 2006 Elsevier B.V. All rights reserved.
doi:10.1016/j.jpowsour.2006.10.093

these have mainly concentrated on electrolyte self-supported or anode-supported cells. This could be primarily attributed to the difficulties of fabricating a dense ceria thin-film on a porous cathode.

Cathode-supported cells like the tubular cell used in the Westinghouse concept, are particularly attractive due to their feasibility for current collecting for stacks. This study thus aims at fabrication and characterization of a cathode-supported cell though a slurry coating/co-firing process, which is a cost effective technology, with a specific interest to use the $La_{0.6}Sr_{0.4}Co_{0.2}Fe_{0.8}O_{3-\delta}$/$Ce_{0.9}Gd_{0.1}O_{1.95}$ couple for low-temperature operation.

2. Experimental

2.1. Sintering investigation of the cell components

Powder characteristics for the cell components are summarized in Table 1. The $Ce_{0.9}Gd_{0.1}O_{1.95}$ (10 mol% gadolinium-doped ceria, GDC) powders were synthesized in two different ways and described simply here:

(1) Coprecipitation method [26]: Ce^{3+} and Gd^{3+} nitrite standard aqueous solution (99.9%, Rhodia, France) was mixed in a selected proportion and then poured into a NH_4HCO_3 (extra pure regent, Wako Pure Chem. Ltd., Japan) water solution. Solution stirring was kept for 3 h at 80 °C. After filtration, the precipitate was dried and calcined at 700 °C for 5 h.
(2) Conventional citrate coprecipitation method: Ce^{3+} and Gd^{3+} carbonates aqueous solution (99.9%, Seimi Chem. Co. Ltd., Japan) was mixed in a selected proportion and citric acid and ethylene glycol were added. The solution was stirred for 3 h at 80 °C to form a homogeneous chelate between the metal cations and the citrate anions. The products were gradually dried and then fired at 600–1000 °C for 5 h to obtain the GDC powders with specific surface areas of 10, 30, 39 $m^2\,g^{-1}$.

As previously revealed, compared with the conventional citrate preparation, the coprecipitation method is capable of yielding $Ce_{0.9}Gd_{0.1}O_{1.95}$ powders with a comparable densification accompanied with a relatively low shrinkage [26]. The $La_{0.6}Sr_{0.4}Co_{0.2}Fe_{0.8}O_{3-\delta}$ (LSCF) powders were prepared from carbonates of each element by a citrate method similar with the $Ce_{0.9}Gd_{0.1}O_{1.95}$. The powders were obtained after calcination of 900 °C for 5 h and further ball-milled for 48 h. NiO–$Ce_{0.9}Gd_{0.1}O_{1.95}$ (Ni to GDC: 50:50, vol.% after reduction) powders were synthesized by a citrate method using Ce^{3+} and Gd^{3+} carbonates and Ni^{2+} nitrite (Kanto Chemical. Co. Inc., Japan) aqueous solution similar with the GDC and LSCF described above. The powders were obtained after calcinations of 700 °C for 5 h. All the as-obtained powders were confirmed by powdered X-ray diffraction (XRD, MacScience M18XHF, Japan); their compositions were confirmed by inductively coupled plasma (ICP) analysis, and specific surface areas were measured by BET (Brunauer–Emmett–Teller) absorption isotherm method using N_2 gas.

To investigate sintering characteristics, the as-prepared powders were pressed to discs in 20 mm diameter and 2–3 mm thickness by uniaxial dry pressing at 200 MPa. This was followed by sintering at selected temperatures over the 600–1200 °C range with a heating rate of 3.3 °C min^{-1}. The dimensions and weight of the unfired and sintered discs were measured to determine the bulk density and the shrinkage. The theoretical density was calculated using the theoretical value determined from the experimental lattice parameters and unit formula based on XRD. The relatively density was derived from a ratio of bulk density to theoretical. The shrinkage of the discs was determined as $(d_1 - d_2)/d_1$, where d_1 and d_2 are initial and final diameter, respectively. The microstructure of the sintered samples was recorded by scanning electron microscopy (SEM, Hitachi, S-3500H, Japan).

2.2. Conductivity and thermal expansion measurements

Electrical conductivity was measured by the four-terminal method. The sintered samples were cut into rectangular bars of approximately 4 mm × 4 mm × 13 mm dimensions. The potential and current leads were contacted by applying platinum paste and fixing to metallic platinum. The thermal expansion was measured in air from 50 to 650 °C using a Mac Science TG-DTA 5000S system using sintered rectangular shapes of 20 mm × 5 mm × 5 mm. A heating/cooling rate was 5 °C min^{-1}, with a 5 min annealing time at maximum temperature.

2.3. Fabrication of the co-fired cell

Preparation of the cathode substrates was as follows: $La_{0.6}Sr_{0.4}Co_{0.2}Fe_{0.8}O_{3-\delta}$ and $Ce_{0.9}Gd_{0.1}O_{1.95}$ powders in the

Table 1
Powders characteristics for the cell components

	Average particle size, D_{50} (μm)	Specific surface area ($m^2\,g^{-1}$)	Theoretical density ($g\,cm^{-3}$)	Preparations	As cell components
$La_{0.6}Sr_{0.4}Co_{0.2}Fe_{0.8}O_{3-\delta}$	0.5	9	6.33	Citrate method	Cathode
$Ce_{0.9}Gd_{0.1}O_{1.95}$	0.22	30	7.214	Newly devised low-temperature process in coprecipitation [26]	Electrolyte
	0.66	39	7.227	Citrate method	Cathode
NiO–$Ce_{0.9}Gd_{0.1}O_{1.95}$ (Ni:GDC: 50:50, vol.% after reduction)	0.4	14	7.005	Citrate method	Anode

desired volumetric ratio were mixed with ethyl cellulose and graphite powders (both from Kanto Chemical. Co. Inc., Japan) and ball-milled with water for 24 h. The mixtures were dried and then uniaxially pressed into discs with 200 MPa to mold the supports. The electrolyte slurry was prepared by ball-milling. The mixture of the $Ce_{0.9}Gd_{0.1}O_{1.95}$ powder, organic ingredients, such as binder, dispersant and solvents was ball-milled for up to 48 h. This slurry was then coated to the cathode substrates. After casting, the tapes were allowed to dry gradually in air for 12 h at room temperature. Finally, the bi-layers of cathode substrate and $Ce_{0.9}Gd_{0.1}O_{1.95}$ were co-fired at 1200 °C for 10 h. The heating and cooling rates were 2.9 and 5 °C min^{-1}, respectively. The anode slurry consisting of NiO–$Ce_{0.9}Gd_{0.1}O_{1.95}$ powder and organic ingredients was prepared in a way analogous with the electrolyte. The anode slurry was coated on the sintered bi-layers and co-fired at 1100 °C for 1 h. The dimensions of the resulting cells were 16 mm diameter × 2.0 mm thickness and the effective anode area was 1 cm^2.

2.4. Cell characterization

Pt meshes were used as current collectors and attached to the electrodes with Pt paste and fixed with a ceramic binder. The cells were connected to a gas manifold and then placed in an oven. The anode and cathode compartments were separately sealed by melting a glass ring gasket at 900 °C. Hydrogen (saturated with H_2O vapor at 20 °C) and air gases were supplied to the anode and cathode compartments, respectively. A flow rate of 50 ml min^{-1} was used for both gases. The tests were carried out in the temperature range from 450 to 600 °C. No gas leakage in the electrochemical measurements was confirmed using bubble-type gas flow meter.

3. Results and discussion

3.1. Sintering characteristics of $La_{0.6}Sr_{0.4}Co_{0.2}Fe_{0.8}O_{3-\delta}$

Sintering characteristics of $La_{0.6}Sr_{0.4}Co_{0.2}Fe_{0.8}O_{3-\delta}$ have been seldom discussed in a temperature range over 1200 °C, since fabrications of such cathodes are usually made at a lower temperature to prevent particles from agglomeration and to avoid a potential interfacial reaction during co-firing with the electrolyte [23–25]. Sintering temperatures play a vital role in the microstructure and densification of the $La_{0.6}Sr_{0.4}Co_{0.2}Fe_{0.8}O_{3-\delta}$ powders was found very speedy, finishing within 1200 °C, as shown in Fig. 1a and b. This densification was retarded to some degree by adding some pore formers (see Fig. 1c). However, with increasing temperature to 1300 °C, a highly dense and pore-free microstructure shown in Fig. 1d was obtained. Although the mixed conducting $La_{0.6}Sr_{0.4}Co_{0.2}Fe_{0.8}O_{3-\delta}$ tends to extend the active area beyond the electrode/electrolyte interface, the fast densification will significantly reduce the three-phase-boundary (TPB) regions as a result of severe particle agglomeration. This raises critical selection of the electrolyte powders, which are expected to have comparable sintering characteristics with the $La_{0.6}Sr_{0.4}Co_{0.2}Fe_{0.8}O_{3-\delta}$ in the co-firing region.

3.2. Selection of $Ce_{0.9}Gd_{0.1}O_{1.95}$ powders

Fig. 2 shows the sintering behavior of the as-obtained $Ce_{0.9}Gd_{0.1}O_{1.95}$ powders; the relatively density and the shrinkage were plotted as a function of temperature in Fig. 2a and b, respectively. As can be seen, due to the enhanced surface solid-state diffusion, a larger specific surface area resulted in a higher shrinkage followed by faster densification. However, it is appar-

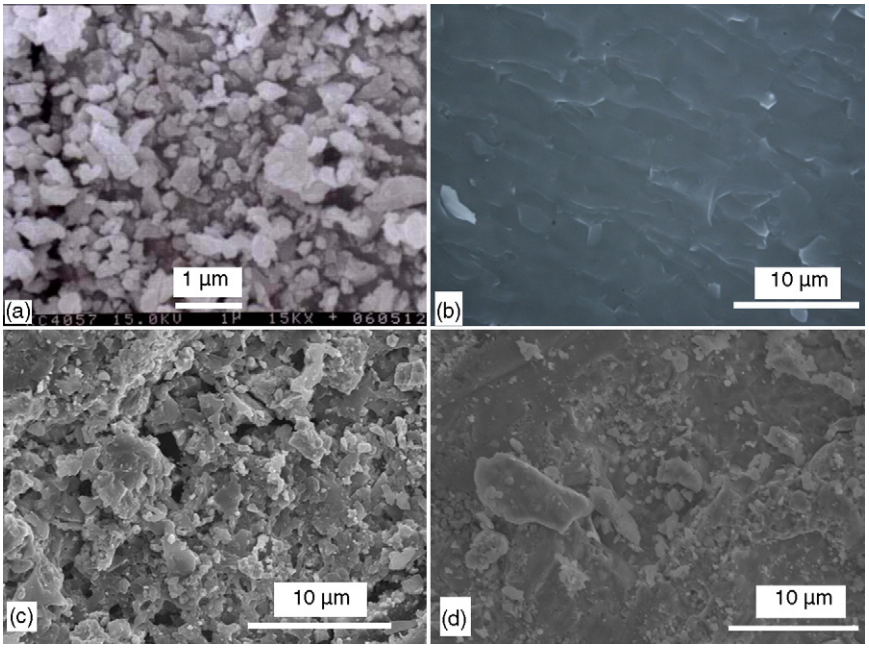

Fig. 1. SEM micrographs of the $La_{0.6}Sr_{0.4}Co_{0.2}Fe_{0.8}O_{3-\delta}$ powders sintered at different temperatures for 10 h: (a) before, (b) 1200 °C, (c) adding of 12 wt.% graphite at 1200 °C, and (d) adding of 12 wt.% graphite at 1300 °C.

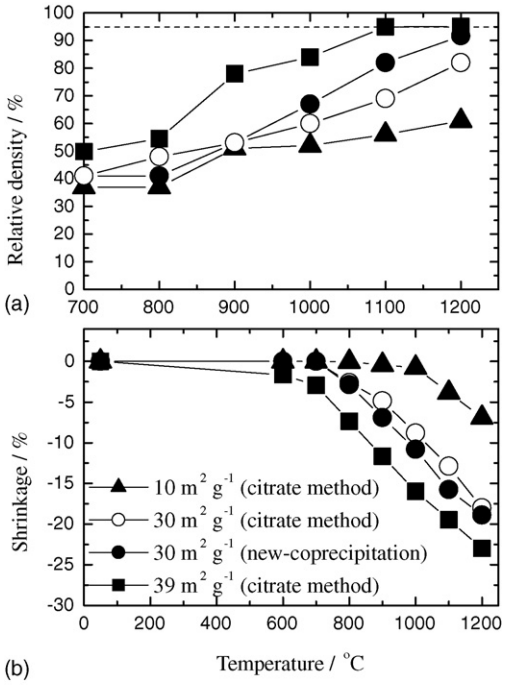

Fig. 2. Temperature change as a function of: (a) relative density (dotted line was plotted to highlight the relative density of 95%) and (b) shrinkage of different $Ce_{0.9}Gd_{0.1}O_{1.95}$ powders.

ent that the powder ($30\,m^2\,g^{-1}$) prepared by the newly devised coprecipitation had a superior sinterability compared to the one with a similar surface area synthesized using the citrate method, postulated as being caused by the powder shape and particle size distribution. The microstructure from TEM micrographs shown in Fig. 3 revealed that the newly devised coprecipitation prepared nano-$Ce_{0.9}Gd_{0.1}O_{1.95}$ has a spherical and dispersible shape, whereas the citrate prepared powder contains many severe particle agglomerations. The latter makes pore-formation easily in the green body during sintering and retards the densification, and thus limits the sinterability of the powder. The high density of ≥92% and ≥95% of theoretical reached at 1200 °C for 0 h for the powder with $30\,m^2\,g^{-1}$ using newly devised coprecipitation and the $39\,m^2\,g^{-1}$ one by citrate method, respectively. Increase in the holding time to 10 h at 1200 °C gave rise to densification for both nano-powders with a relative density >98%. This suggested a potentially low co-firing temperature of 1200 °C via the use of the nano-$Ce_{0.9}Gd_{0.1}O_{1.95}$ proposed.

3.3. Shrinkage control in the cathode substrate

Compared to the nano-$Ce_{0.9}Gd_{0.1}O_{1.95}$ powders, the shrinkage of the $La_{0.6}Sr_{0.4}Co_{0.2}Fe_{0.8}O_{-\delta}$ did not follow the densification and appeared slower for ca. 5–10% in the temperature range from 800 to 1200 °C, as shown in Fig. 4a. In order to favor the shrinkage of the $La_{0.6}Sr_{0.4}Co_{0.2}Fe_{0.8}O_{3-\delta}$, nano-$Ce_{0.9}Gd_{0.1}O_{1.95}$ powders were added. The $Ce_{0.9}Gd_{0.1}O_{1.95}$ with specific surface area of $39\,m^2\,g^{-1}$ prepared by the citrate method was very effective because of a higher surface activity. Fine scale materials of $Ce_{0.9}Gd_{0.1}O_{1.95}$ are further expected to improve the TPB area leading to a low cathodic polarization. For such composites, 30–40 wt.% of gadolinium-doped ceria was reported as being optimal for improving the electrochemical performance [11,27]. In the present research, adding the $Ce_{0.9}Gd_{0.1}O_{1.95}$ with a surface area of $39\,m^2\,g^{-1}$ to the $La_{0.6}Sr_{0.4}Co_{0.2}Fe_{0.8}O_{3-\delta}$ with a volumetric ratio of 30% and 40% (ca. 33 and 43 wt.%) yielded a high shrinkage of 20%, which was still lower than that of the nano-$Ce_{0.9}Gd_{0.1}O_{1.95}$ with surface area of $39\,m^2\,g^{-1}$ prepared by the citrate method but was comparable to the $30\,m^2\,g^{-1}$ one synthesized using the newly devised coprecipitation. The latter was then selected as the electrolyte to match the substrate in the sintering profiles, as shown in Fig. 4b. If the support cathode is made to dominate and assist the densification of the supported electrolyte film during co-firing, then the full density for the electrolyte film should be reached at approximately 1200 °C.

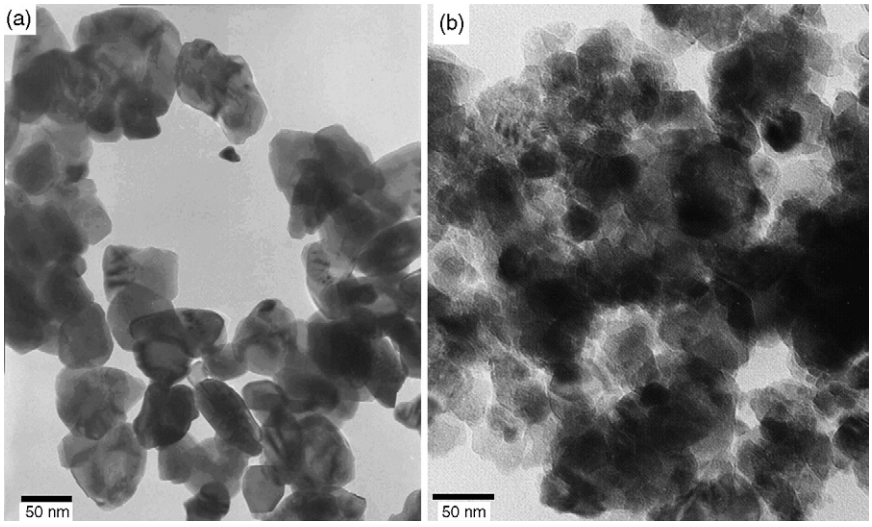

Fig. 3. TEM micrographs of the $Ce_{0.9}Gd_{0.1}O_{1.95}$ nano-powders with specific surface area of $30\,m^2\,g^{-1}$ synthesized using (a) newly devised low-temperature process in coprecipitation and (b) citrate method using carbonates.

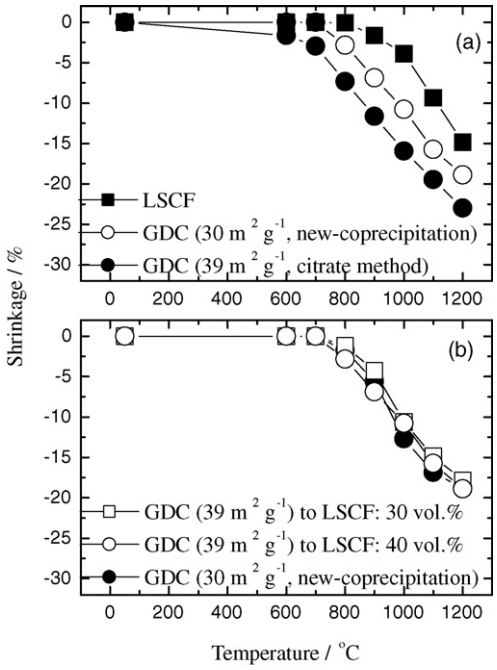

Fig. 4. Shrinkage profiles of: (a) $La_{0.6}Sr_{0.4}Co_{0.2}Fe_{0.8}O_{3-\delta}$ and nano-$Ce_{0.9}Gd_{0.1}O_{1.95}$ powders; (b) the nano-$Ce_{0.9}Gd_{0.1}O_{1.95}$ ($30\,m^2\,g^{-1}$ as electrolyte) and the composites after adding of nano-$Ce_{0.9}Gd_{0.1}O_{1.95}$ ($39\,m^2\,g^{-1}$) to $La_{0.6}Sr_{0.4}Co_{0.2}Fe_{0.8}O_{3-\delta}$ (in 30 and 40 vol.%).

3.4. Morphological modification of the cathode substrate

For the cathode-supported SOFCs, the porosity of the sintered cathode substrate has to be optimized for O_2 diffusion due to a mass transportation limitations. Therefore, the effect of changing the amount and identity of the pore former on both the shrinkage and relatively density of the substrates was studied, as shown in Fig. 5. As expected, the relatively density, which potentially indicates a residual porosity, decreased with increasing amounts of pore formers, while maintaining a necessary linear shrinkage. It was found that the influence of graphite powders on the shrinkage was slightly higher than ethyl cellulose, but this was contradictory in producing porosity. This is partly attributed to the decomposition temperature, $\leq$800 °C for graphite and $\leq$500 °C for ethyl cellulose.

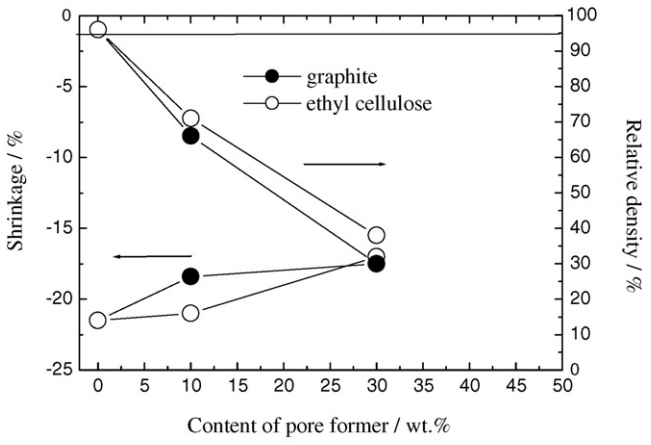

Fig. 5. Shrinkage profiles and relative density of the cathode substrates based on $La_{0.6}Sr_{0.4}Co_{0.2}Fe_{0.8}O_{3-\delta}$ and nano-$Ce_{0.9}Gd_{0.1}O_{1.95}$ (60:40, vol.%) sintered at 1200 °C as a function of pore formers (relative density of 95% was plotted).

Fig. 6 further shows cross-sectional SEM micrographs of the composite substrates after sintering at 1200 °C for 10 h as a function of pore formers. Dense and pore-free bodies without any pore former shown in Fig. 6a make it difficult for gas to diffuse through the thick cathode. Comparing two porous samples, one with a non-uniform and partially closed porosity (ethyl cellulose, Fig. 6b), the other with a uniform and connected porosity (graphite, Fig. 6c) made the fine graphite powders competitive as fore formers. A possibly strong particle agglomeration, which was caused by a high viscosity of ethyl cellulose dissolved with water, to some degree, could be the consequence. However, ethyl cellulose was found very effective to mold the substrates and prevent the as-coated electrolyte slurry from peeling off the as-prepared discs prior to sintering. Therefore, 12 wt.% of ethyl cellulose plus 15 wt.% of graphite relative to ceramic (ca. 50 vol.%) was chosen and gave the substrates homogeneous and continuous pores, as shown in Fig. 6d. This result is consistent with that reported previously by Corbin and Apte [28] and shows that graphite powders mixed with polymer are effective in producing porosity without altering shrinkage characteristics. Optimizing sintering properties and sintered microstructure makes it possible to laminate a dense GDC thin-film to compatible with a porous LSCF–CGO substrate and co-firing at 1200 °C without introducing undue stress or cracks in either layer.

3.5. Electrical conductivity and thermal expansion behaviors of the $La_{0.6}Sr_{0.4}Co_{0.2}Fe_{0.8}O_{3-\delta}$ based cathodes

Fig. 7 shows the electrical conductivity of the sintered porous $La_{0.6}Sr_{0.4}Co_{0.2}Fe_{0.8}O_{3-\delta}$–$Ce_{0.9}Gd_{0.1}O_{1.95}$ bodies (porosity of ca. 50%) as a function of temperature. For comparison, the $La_{0.6}Sr_{0.4}Co_{0.2}Fe_{0.8}O_{3-\delta}$ powders were sintered at 1200 °C for 10 h to have a density greater than 95% of theoretical. The conductivity of such dense $La_{0.6}Sr_{0.4}Co_{0.2}Fe_{0.8}O_{3-\delta}$ gradually increases up to 600 °C and then slightly decreases. This decrease in the conductivity is attributed to the increase in oxygen nonstoichiometry arising from a decrease in the concentration of p-type charge carriers at high temperatures [16]. At room temperature, $La_{0.6}Sr_{0.4}Co_{0.2}Fe_{0.8}O_{3-\delta}$ is stoichiometric and becomes nonstoichiometric at $T > 600$ °C [16–19]. The porous $La_{0.6}Sr_{0.4}Co_{0.2}Fe_{0.8}O_{3-\delta}$ had an electrical conductivity two and a half times smaller than the dense one, and this decrease could be explained by the difference in the charge carriers (O^{2-} ions and electrons) in a dense or porous body, which is strongly influenced by the microstructure and sintering conditions [29]. The electrical conductivity further decreased with addition of $Ce_{0.9}Gd_{0.1}O_{1.95}$ to the porous $La_{0.6}Sr_{0.4}Co_{0.2}Fe_{0.8}O_3$. However, it is obvious that change in the $Ce_{0.9}Gd_{0.1}O_{1.95}$ content is negligibly small in a porous body suggesting that the optimum $Ce_{0.9}Gd_{0.1}O_{1.95}$ content in a porous structure would have a lower influence on the conductivity but higher on the electrode overpotential [27].

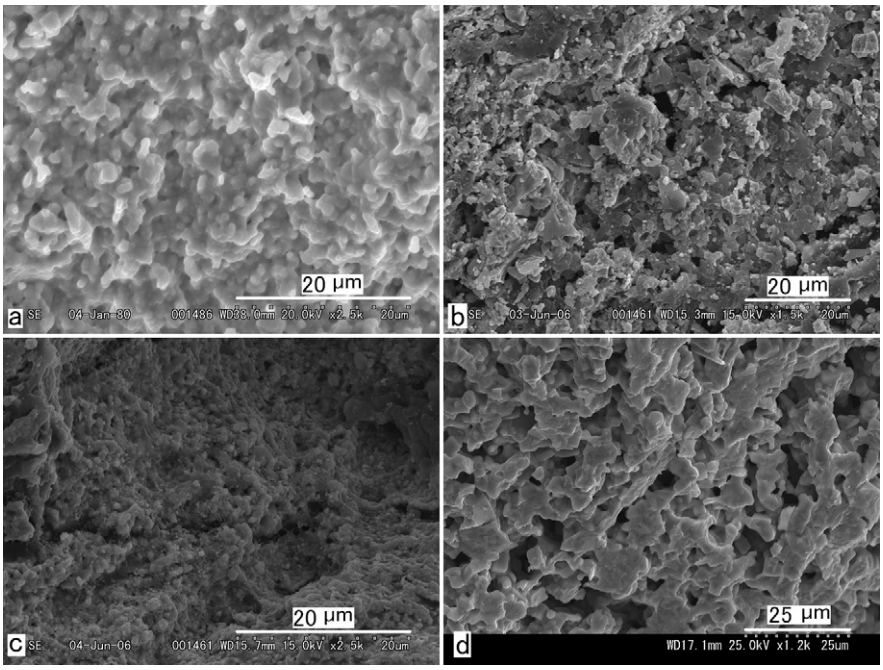

Fig. 6. Cross-section SEM micrographs of the substrates based on $La_{0.6}Sr_{0.4}Co_{0.2}Fe_{0.8}O_{3-\delta}$ and nano-$Ce_{0.9}Gd_{0.1}O_{1.95}$ (60:40, vol.%) after sintering at 1200 °C as a function of pore formers of: (a) without, (b) 12 wt.% ethyl cellulose, (c) 12 wt.% graphite, and (d) 15 wt.% graphite plus 12 wt.% ethyl cellulose.

Fig. 8a shows the thermal expansion behavior of the $La_{0.6}Sr_{0.4}Co_{0.2}Fe_{0.8}O_{3-\delta}$ based substrates as a function of the $Ce_{0.9}Gd_{0.1}O_{1.95}$ contents in air; their thermal expansion coefficients from 50 to 600 °C were summarized in Fig. 8b. To reflect a real situation, the $La_{0.6}Sr_{0.4}Co_{0.2}Fe_{0.8}O_{3-\delta}$ based composites were sintered at 1200 °C with pore formers to have a porosity of ca. 50%, whereas the dense $Ce_{0.9}Gd_{0.1}O_{1.95}$ was obtained with a full density over 95% of the theoretical. With a porous microstructure, the thermal expansion behavior was dominated by $La_{0.6}Sr_{0.4}Co_{0.2}Fe_{0.8}O_{3-\delta}$ and was independent of the $Ce_{0.9}Gd_{0.1}O_{1.95}$ content. Porous samples with various $Ce_{0.9}Gd_{0.1}O_{1.95}$ contents showed coincident thermal expansions comparable to dense $Ce_{0.9}Gd_{0.1}O_{1.95}$ with a <0.15% difference at ≤700 °C (see Fig. 8a). The thermal expansion coefficient (TEC) of the dense $La_{0.6}Sr_{0.4}Co_{0.2}Fe_{0.8}O_{3-\delta}$ was (14–15) × 10^{-6} °C^{-1} as compared to (11–12) × 10^{-6} °C^{-1} for the dense $Ce_{0.9}Gd_{0.1}O_{1.95}$, but decreased to about (12–13) × 10^{-6} °C^{-1} for the porous $La_{0.6}Sr_{0.4}Co_{0.2}Fe_{0.8}O_{3-\delta}$ and further (11.5–12) × 10^{-6} °C^{-1} for the porous LSCF–GDC composites. This suggested that the porous cathodes highly alle-

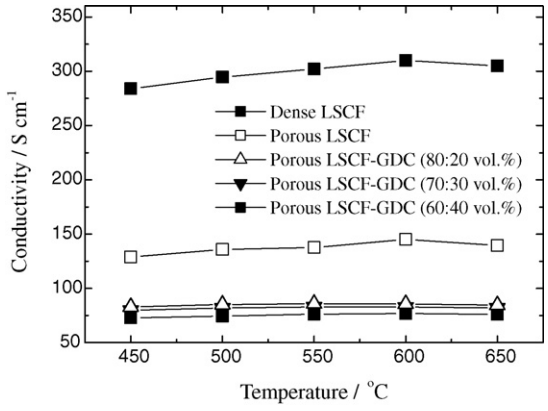

Fig. 7. Electrical conductivity of the porous cathode substrates with different $Ce_{0.9}Gd_{0.1}O_{1.95}$ contents in comparison to dense and porous $La_{0.6}Sr_{0.4}Co_{0.2}Fe_{0.8}O_{3-\delta}$.

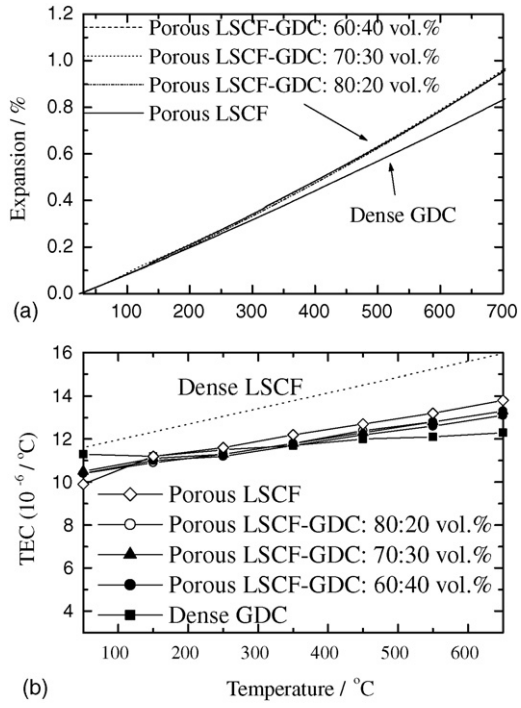

Fig. 8. Thermal expansion behavior of: (a) porous cathode substrates with different $Ce_{0.9}Gd_{0.1}O_{1.95}$ contents compared with dense $La_{0.6}Sr_{0.4}Co_{0.2}Fe_{0.8}O_{3-\delta}$ and $Ce_{0.9}Gd_{0.1}O_{1.95}$ and (b) thermal expansion coefficients.

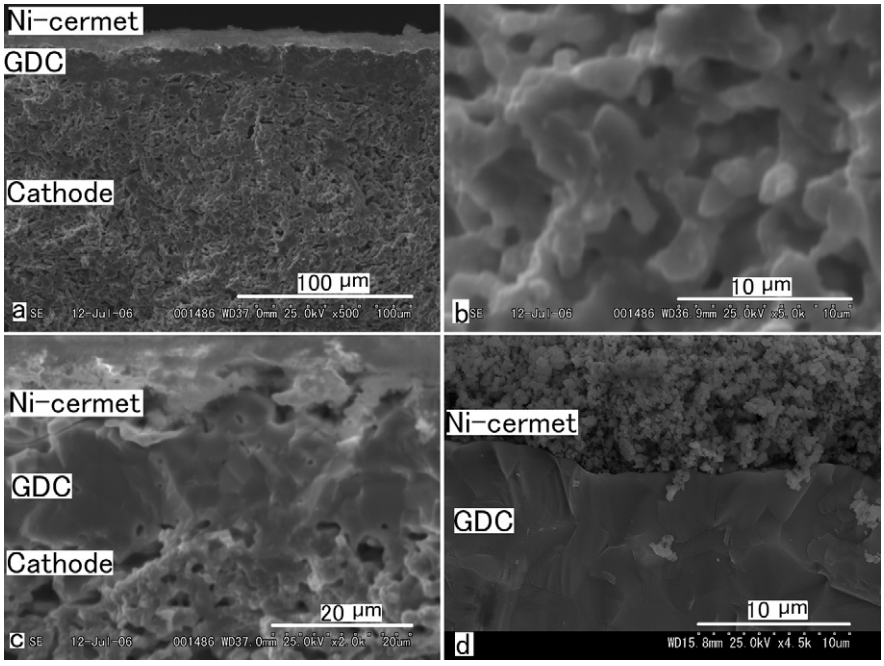

Fig. 9. Cross-section SEM micrographs of: (a) the co-fired cathode-supported cell, the enlarged images of (b) substrate, (c) cathode/electrolyte/anode interface, and (d) anode/electrolyte layer after reduction.

viate the thermal expansion of $La_{0.6}Sr_{0.4}Co_{0.2}Fe_{0.8}O_{3-\delta}$ and thus are suitable substrates for $Ce_{0.9}Gd_{0.1}O_{1.95}$ electrolytes.

3.6. Fabrication of a co-fired cell

Fig. 9a shows a typical laboratory-sized cell including a dense $Ce_{0.9}Gd_{0.1}O_{1.95}$ thin-film between a porous LSCF/GDC substrate (bottom) and a porous thin NiO–GDC layer (top). The thickness was about 15 μm for the electrolyte membrane and 10 μm for the anode. The substrate contained 15 wt.% graphite and 12 wt.% cellulose and its relative density was ca. <50% after sintering, indicating a porosity of over 50%. The morphology of the substrate shown in Fig. 9b was relatively uniform suggesting that the pore formers were homogeneously distributed throughout the substrate prior to sintering. The two oxides were not separated completely from each other, but were an agglomerated mixture. Fig. 9c further shows the cathode and anode layers near the electrolyte where most of the electrochemical reaction occurs. There was good adhesion at both the anode–electrolyte and electrolyte–cathode interfaces. For such a co-fired configuration, the electrode microstructure and activity depended strongly on the co-firing temperature for the cell components, e.g. ≤1200 °C for LSCF–GDC/GDC bi-layers, and <1200 °C for the subsequent NiO–$Ce_{0.9}Gd_{0.1}O_{1.95}$ anode forming. Fine Ni-cermet powers proposed in this study allowed lower sintering temperatures to avoid the destruction of the microstructure of the as-established cathode in the subsequent anode co-firing. In theory, porous mixtures of electro-catalyst and electrolyte materials should increase the TPB line length and lead to an enhanced performance. As compared in Fig. 9d, the microstructure of the cathode substrate (Fig. 9b) was slightly coarser than that of the anode layer, in which reduction of NiO to Ni has beneficial effects to create high porosity. However, mixed conducting $La_{0.6}Sr_{0.4}Co_{0.2}Fe_{0.8}O_{3-\delta}$ might have an extended TPB to lower the influence from such a coarse microstructure.

3.7. Cell performance

For doped ceria electrolytes, it is widely accepted that reducing operating temperature (<600 °C) and increasing the P_{O_2} in fuel are effective to suppress the partial reduction of Ce^{4+} in order to achieve a high open circuit voltage (OCV) [4–10]. In a practical low-temperature operation, the thickness of the ceria membrane has to be as low as possible. Fig. 10 shows the OCV as a function of the operating temperature of the as-proposed cells in association with the thickness of the $Ce_{0.9}Gd_{0.1}O_{1.95}$ membrane. For comparison, $Ce_{0.9}Gd_{0.1}O_{1.95}$ self-supported cells

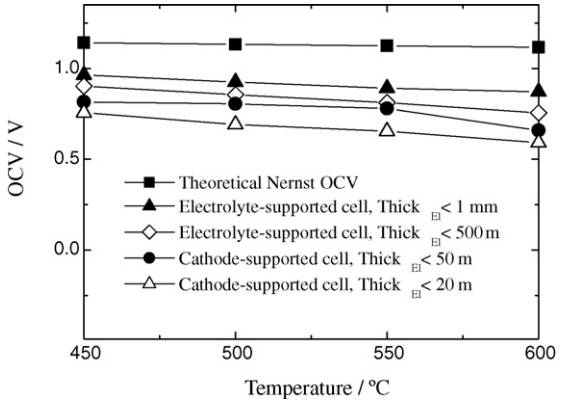

Fig. 10. Open circuit voltage as a function of operating temperature of the co-fired cells in association with the cell design and thickness of $Ce_{0.9}Gd_{0.1}O_{1.95}$ membrane.

with an electrolyte thickness of ≤500 μm and ≤1 mm were fabricated. As can be seen, the decrease in electrolyte thickness and the increase in operating temperature gave a noticeable increase in the unexpected OCV drops. This could be explained by a decrease in resistance for migration of the charge carriers (O^{2-} ions and electrons) in ceria which tends to increase the internal short circuit current [9,10]. The OCV for the self-supported ceria with thickness of 950 μm was ca. 0.95 V at 500 °C, 0.92 V at 550 °C, and 0.9 V at 600 °C, which are comparable to the values in several publications [6,9,10]. Thinner electrolyte membranes, e.g. ≤50 and ≤20 μm, further obviously decreased the OCVs for the cathode-supported cells. A previous report by Gödickemeier and Gauckler [6] revealed that, to ensure a high OCV, the optimum thickness of electrolyte with mixed conductivity requires a selection in the electrode pairs. More recently, Ogumi et al. [9,10] reported that the OCV of ceria electrolytes is dependent on electrode activity and electrolyte thickness. These results agree well with the present results. That is, due to an internal short circuit current caused by the mixed conductivity of ceria, the overpotentials at the electrode/electrolyte interfaces related with the cell design and electrode microstructure affect the OCV, and such influences become stronger the thinner the electrolyte. It is suggested that, in addition to ceria, a modification in the cell design, such as the cathode microstructure in case of this research, could yield optimum efficiency and power output from a practical point of view.

Furthermore, the interfacial reaction associated with elemental diffusion from $La_{0.6}Sr_{0.4}Co_{0.2}Fe_{0.8}O_{3-\delta}$ to $Ce_{0.9}Gd_{0.1}O_{1.95}$ tends to cause microstructural degradation of the electrolyte during co-sintering of the electrolyte and cathode and could potentially influence the OCV. Fig. 11 shows a cross-sectional SEM micrograph and elemental distribution of the co-fired cathode-supported $Ce_{0.9}Gd_{0.1}O_{1.95}$ cell. Small traces of transition metals of Co and Fe (<2 mol%, as confirmed by energy dispersive X-ray analysis, EDX) were found in the electrolyte layer. Small additions (<2 mol%) of transition metal oxides into the doped ceria have been reported to considerably favor densification [14,30,31]. This could be explained by formation of an amorphous transition metal rich grain boundary film that facilitates the densification via a liquid phase with a minimum of grain growth. The minor dopant additions have no essential effect on the total and ionic conductivity, but considerably increase the p-type electronic transport [14]. A further investigation regarding such influences on the thinner electrolyte membrane (e.g. <50 μm) associated with the electrode microstructure and optimization of the co-firing conditions remain to be done.

Fig. 12 shows the power and *j–V* performance of a cathode-supported cell at 550 and 600 °C. The maximum power density obtained was 35 mW cm^{-2} at 550 °C, 60 mW cm^{-2} at 600 °C. The cell polarization curves were almost linear in a low current density range and the power drop after the peak was characteristic of a gas diffusion limitation. The cell performance could be affected by various parameters, especially the gas-diffusion activity of the cathodes (or the porosity), the degree of fineness of the cathode microstructure and the thickness of the porous cathode substrate. These greatly hinder the power densities of the cell being benefited from the good combination of the LSCF/GDC. It is suggested that further work should lead to the modification of cell construction, particularly in the support electrode microstructure, thickness, or electrode/electrolyte interface associated with cathode polar-

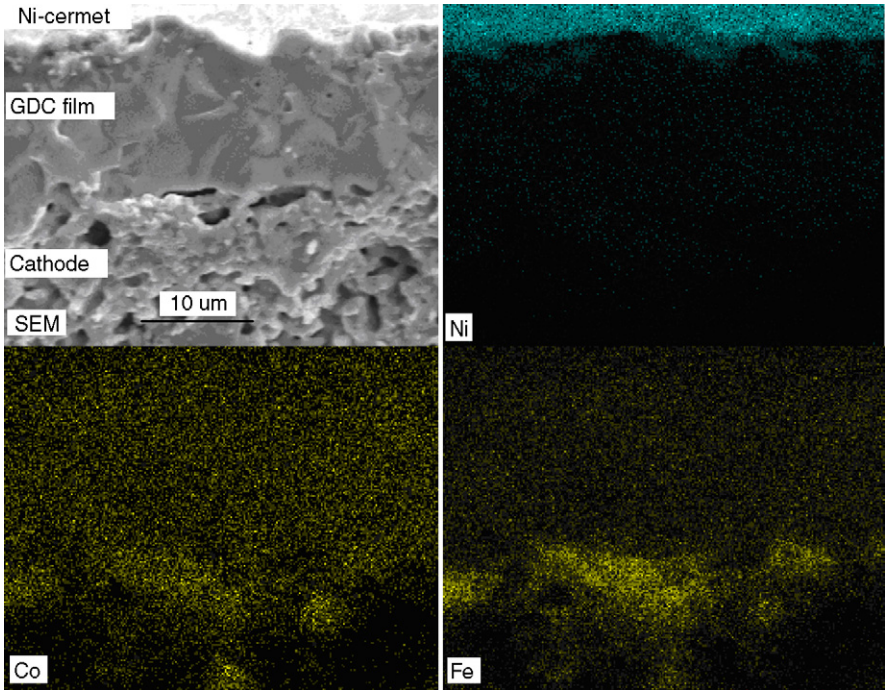

Fig. 11. Cross-section SEM micrograph and elemental distribution of the co-fired cathode-supported cell: SEM, and elemental map of Ni, Co, and Fe.

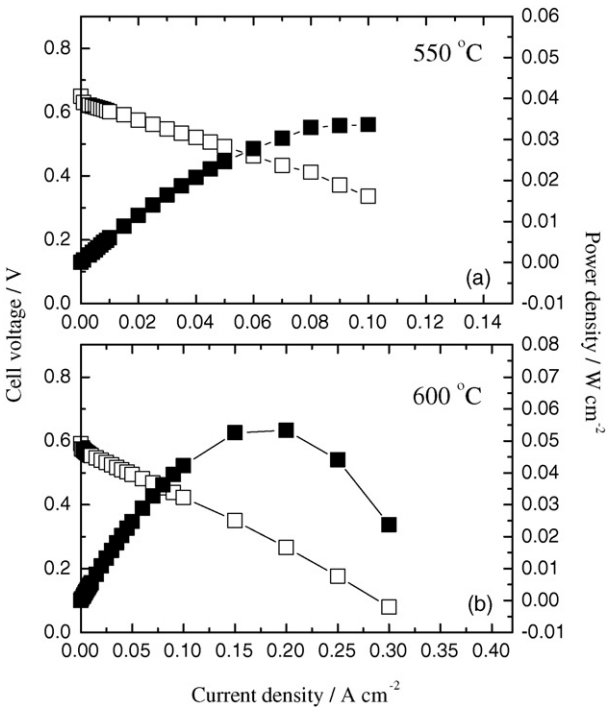

Fig. 12. Current–voltage and power density characteristics of a co-fired cathode-supported cell at 550 and 600 °C.

ization. Furthermore, the OCVs obtained here are relatively low due to the use of a ceria-based electrolyte. This could be resolved to some degree by optimization of the sintering conditions and by some other solutions suggested by different authors [7–10,32,33].

4. Conclusions

The fabrication and characterization of a $La_{0.6}Sr_{0.4}Co_{0.2}Fe_{0.8}O_{3-\delta}$ cathode-supported $Ce_{0.9}Gd_{0.1}O_{1.95}$ thin-film cell via a slurry coating/co-firing process were investigated. Nano-$Ce_{0.9}Gd_{0.1}O_{1.95}$ powder with a surface area of $30\,m^2\,g^{-1}$ was prepared by a newly devised coprecipitation method as a low-temperature sinterable electrolyte, whereas $39\,m^2\,g^{-1}$ nano-$Ce_{0.9}Gd_{0.1}O_{1.95}$ synthesized by the citrate method was added to the $La_{0.6}Sr_{0.4}Co_{0.2}Fe_{0.8}O_{3-\delta}$ to favor matching of shrinkage of the cathode substrate with the supporting membrane. Such a combination was found to greatly assist the densification of the doped ceria membrane without introducing any cracks and deformations. Co-firing of the bi-layers of cathode/electrolyte and a subsequent Ni-cermet forming were successful at 1200 and at 1100 °C, respectively. A laboratory-sized tri-layer cell, not yet optimized for performance, was shown to be feasible operating below 600 °C fed with humidified H_2 (3 wt.% H_2O), and the maximum power density obtained was $35\,mW\,cm^{-2}$ at 550 °C, $60\,mW\,cm^{-2}$ at 600 °C.

Acknowledgement

This work has been supported by NEDO, Japan, as part of the Advanced Ceramic Reactor Project.

References

[1] O. Yamamoto, Electrochim. Acta 45 (2000) 2423.
[2] B.C.H. Steel, Solid State Ionics 75 (1995) 157.
[3] H. Yahiro, K. Eguchi, H. Arai, Solid State Ionics 36 (1989) 71.
[4] H. Inaba, H. Tagawa, Solid State Ionics 83 (1996) 1.
[5] M. Mogensen, N.M. Sammes, G.A. Tompsett, Solid State Ionics 129 (2000) 63.
[6] M. Gödickemeier, L.J. Gauckler, J. Electrochem. Soc. 145 (1999) 414.
[7] D.L. Maricl, et al., Solid State Ionics 52 (1992) 173.
[8] K. Eguchi, T. Setoguchi, T. Inoue, H. Arai, Solid State Ionics 52 (1992) 165.
[9] T. Mastui, M. Inaba, A. Mineshige, Z. Ogumi, Solid State Ionics 176 (2005) 647.
[10] M. Inaba Kosaka, A. Mineshige, Z. Ogumi, Solid State Ionics 176 (2005) 663.
[11] B.C.H. Steele, Solid State Ionics 129 (2000) 95.
[12] J. Ma, T.S. Zhang, L.B. Kong, P. Hing, S.H. Chan, J. Power Sources 132 (2004) 71.
[13] T.S. Zhang, J. Ma, L.B. Kong, P. Hing, Y.J. Leng, S.H. Chan, J.A. Kilner, J. Power Sources 124 (2003) 26.
[14] K.R. Reddy, K. Karan, J. Electroceram. 15 (2005) 45.
[15] R.S. Torrens, N.M. Sammes, G.A. Tompsett, Solid State Ionics 111 (1998) 9.
[16] L.W. Tai, et al., Solid State Ionics 75 (1995) 273;
L.W. Tai, et al., Solid State Ionics 76 (1995) 259.
[17] S.B. Adler, J.A. Lane, B.C.H. Steele, J. Electrochem. Soc. 143 (1996) 3554.
[18] L.W. Tai, M.M. Nasralla, H.U. Anderson, in: S.C. Singhal, H. Iwahara (Eds.), Proceedings of the Third International Symposium on Solid Oxide Fuel Cells, The Electrochemical Society Proceedings Series, Pennington, NJ, 1999, p. 241.
[19] C.C. Chen, M.M. Nasralla, H.U. Anderson, in: S.C. Singhal, H. Iwahara (Eds.), Proceedings of the Third International Symposium on Solid Oxide Fuel Cells, The Electrochemical Society Proceedings Series, Pennington, NJ, 1999, p. 252.
[20] E.P. Murray, M.J. Sever, S.A. Barnett, Solid State Ionics 148 (2002) 27.
[21] S.J. Visco, C. Jacobson, L.C. De Jonhe, in: U. Stimming, S.C. Singhal, H. Tagawa, W. Lehnert (Eds.), Solid Oxide Fuel Cells V, The Electrochemical Society Proceedings Series, Pennington, NJ, 1997, p. 710.
[22] W.G. Wang, M. Mogensen, Solid State Ionics 176 (2005) 457.
[23] R. Doshi, V.L. Richards, J.D. Carter, X. Wang, M. Krumpelt, J. Electrochem. Soc. 146 (1999) 1273.
[24] Y.J. Leng, S.H. Chan, S.P. Jiang, K.A. Khor, Solid State Ionics 170 (2004) 9.
[25] T. Suzuki, T. Yamaguchi, Y. Fujishiro, M. Awano, J. Power Sources 160 (2006) 73.
[26] E. Suda, B. Pacaud, Y. Montardi, M. Mori, M. Ozawa, Y. Takeda, Electrochemistry 71 (2003) 866.
[27] V. Dusastre, J.A. Kiliner, Solid State Ionics 126 (1999) 163.
[28] S.F. Corbin, P.S. Apte, J. Am. Ceram. Soc. 82 (1999) 693.
[29] C. Guizard, A. Julbe, O. Robbe, S. Sarrade, Catal. Today 104 (2005) 120.
[30] D.P. Fagg, V.V. Kharton, J. Frade, J. Electroceram. 9 (2002) 199.
[31] M. Mori, E. Suda, B. Pacaud, K. Murai, T. Moriga, J. Power Sources 157 (2006) 688.
[32] K. Eguchi, T. Setoguchi, T. Inoue, H. Arai, Solid State Ionics 52 (1992) 165.
[33] D. Hirabayashi, A. Tomita, M. Nagao, M. Sano, Electrochem. Solid-State Lett. 10 (2004) A318.